(γ,p), (γ,pn), and (γ,pp) reactions on light nuclei in the $\Delta(1232)$ resonance region

M. Kanazawa, S. Homma, M. Koike, Y. Murata, H. Okuno, F. Soga, and N. Yoshikawa
Institute for Nuclear Study, University of Tokyo, Tokyo 188, Japan

A. Sasaki
Faculty of Education, Akita University, Akita 010, Japan
(Received 30 June 1986)

The cross sections of the reactions (γ,p), (γ,pn), and (γ,pp) are measured for ^{1}H, ^{2}H, ^{9}Be, ^{12}C, and ^{16}O in the $\Delta(1232)$ resonance region by use of a tagged photon beam. Protons emitted at $\theta_p=30°$ are measured by a magnetic spectrometer, and the other neutrons or protons are measured by an array of scintillation counter hodoscopes. From the present experiment, it is concluded that the reactions, $\gamma+$"N"$\rightarrow p+\pi$ and $\gamma+$"pn"$\rightarrow p+n$, contribute dominantly to the (γ,p) reaction in this energy region, where "N" denotes the nucleon and "pn" denotes the pn system in the nucleus.

I. INTRODUCTION

Up to now, data on the photoemission of protons from various nuclei have been accumulated by various authors, especially in the energy region below meson threshold. Since photons were considered to be absorbed by the nucleus mainly through electric dipole in this energy region, the results of the (γ,p) reactions were usually analyzed by use of a quasideuteron model introduced by Levinger.[1]

At energies around 300 MeV, however, it is considered that the photon is absorbed predominantly by the single nucleon to form the $\Delta(1232)$ resonance rather than by the nucleus as a whole. The formed Δ, then, may decay in the nucleus ($\Delta\rightarrow N+\pi$) or interact with a nearby nucleon in the nucleus ($\Delta+N\rightarrow N+N$). As a consequence, it is expected that the nucleon and pion or two nucleons are emitted from the nucleus. Since the probability of the latter mechanism for the photoemission of two nucleons from the nucleus depends strongly on the short range behavior of the nuclear wave function, the reactions (γ,p), (γ,pn), and (γ,pp) in the Δ resonance region are very important in the study of nuclear structure.

Until now, several experiments were performed in this energy region. Before 1970, Barton *et al.*,[2] Garvey *et al.*,[3] and Stein *et al.*[4] measured angular correlations between the proton and the neutron photoemitted from various nuclei by the bremsstrahlung beam. The results of their experiments were analyzed in terms of the quasideuteron model of Levinger[1] or that extended by Gottfried.[5] These phenomenological models explained experimental data qualitatively. However, since these experiments were performed using the bremsstrahlung beam, it was difficult to study the precise mechanism of photoemission of two nucleons from the nucleus.

Recently, a tagged photon beam became available with an energy resolution of about 10 MeV. Several groups[6–8] performed experiments on the (γ,p) reaction by these beams. Among them, Homma *et al.*[7] measured inclusive proton spectra from ^{9}Be and ^{12}C nuclei at the proton laboratory angle of 25°, and observed two peaks which were supposed to be due to the following quasifree reactions,

$$\gamma+\text{"N"}\rightarrow p+\pi \tag{1}$$

and

$$\gamma+\text{"pN"}\rightarrow p+N\ , \tag{2}$$

where "N" denotes a nucleon in the nucleus and "pN" denotes a two-nucleon system in the nucleus ("pn" or "pp"). A coincidence measurement of two nucleons for reactions $A(\gamma,pn)$ and $A(\gamma,pp)$ was first performed by Arends *et al.*[6] for ^{12}C by use of the tagged photon beam in the $\Delta(1232)$ resonance region. They observed the similar angular correlation between the proton and the neutron as in the previous bremsstrahlung experiments. However, since the momentum resolution of this experiment was not accurate enough, it was difficult to extract detailed information on the reaction mechanism.

The purposes of the present experiment are (1) to confirm our previous interpretation[7] on two peaks observed in the inclusive proton momentum spectra for light nuclei, (2) to obtain the basic information on the momentum distribution and the separation energy distribution of the two-nucleon system in the nucleus, (3) to determine the cross sections of the quasifree reactions,

$$\gamma+\text{"pn"}\rightarrow p+n \tag{3}$$

and

$$\gamma+\text{"pp"}\rightarrow p+p\ , \tag{4}$$

separately, and (4) to measure the photon energy dependence and the mass number dependence of cross sections to study the mechanism for quasifree reactions in this energy region.

For these purposes, momenta and emission angles of both nucleons from the reactions (γ,pn) and (γ,pp) were measured together with the incident photon energy. This semiexclusive measurement enabled us to extract the quasifree reaction (2) from the large background due to the quasifree pion photoproduction (1).

In Secs. II and III the overview of the experimental apparatus and the event reconstruction procedure are described. The results of the single-arm and coincidence

measurements are presented in Sec. IV. Discussions are described in Sec. V.

II. EXPERIMENT

The experiment was performed with the use of a tagged photon beam at the 1.3 GeV electron synchrotron, Institute for Nuclear Study, University of Tokyo. The photon energy range covered by the experiment is 187—427 MeV. The targets studied were ^{1}H, ^{2}H, ^{9}Be, ^{12}C, and ^{16}O. The magnetic spectrometer was set at the laboratory angle of 30° to measure the proton from the reactions (γ,p), (γ,pn), and (γ,pp). On the opposite side of the magnetic spectrometer, an array of 64 plastic scintillation counters was set to measure the momentum of the neutron or proton in coincidence with a forward proton. This counter hodoscope covered the laboratory angle from 90° to 170°. The whole experimental setup is shown in Fig. 1.

A. Tagged photon beam

The electron beam was extracted from the 1.3 GeV electron synchrotron with the Piccioni method,[9] and transported to the experimental area through two bending magnets and a pair of quadrupole magnets.

The energy spread of the electron beam transported to the experimental area was 0.3% full width at half maximum (FWHM). The size of the electron beam was about 10 mm (FWHM) in diameter at the radiator position of the photon tagging system.

The photon tagging system consisted of a radiator, an electron analyzing magnet, and a tagging hodoscope consisting of 24 scintillation counters. The photon energy range covered by this tagging system is 240 MeV, which is divided into 24 bins by tagging counters. The resultant photon energy bin is 10 MeV and its resolution is ± 7 MeV. The details of the tagging system are described elsewhere.[10]

B. Targets

The nuclear targets used in the experiment were ^{1}H (hydrogen in water), ^{2}H (liquid deuterium), ^{9}Be (natural beryllium plate), ^{12}C (natural carbon plate), and ^{16}O (oxygen in water).

The liquid deuterium target utilized the CRYODYNE mechanical refrigerator.[11] The cylindrical target container of liquid deuterium was made of Mylar film 127 μm thick, 60 mm in diameter, and 123 mm long. The container of the distilled water was made of Mylar films 127 μm thick, 200 mm in diameter, and 21 mm long. The ^{9}Be and ^{12}C targets were solid plates with sizes of $50\times 70\times 10$ and $100\times 150\times 11$ mm^{3}, respectively.

C. Magnetic spectrometer

A magnetic spectrometer was used to determine the momentum of the protons emitted from the target at the laboratory angle of 30°. The spectrometer, shown in Fig. 1, consists of a bending magnet, three triggering scintillation counters (TF, TM, and TB), and tracking chambers, i.e., multiwire proportional chambers (MWPC's) and drift chambers (DC's). The momentum calibration of the spectrometer was made within an error of less than 1% by use of an extracted electron beam with a momentum of 550 MeV/c. The momentum resolution of the spectrometer (FWHM) was measured to be about 5% at 550 MeV for electrons. The spectrometer was also calibrated with the use of the two-body reaction $\gamma + d \rightarrow p + n$ at $\theta_p = 30°$. The momentum resolution for the protons thus deter-

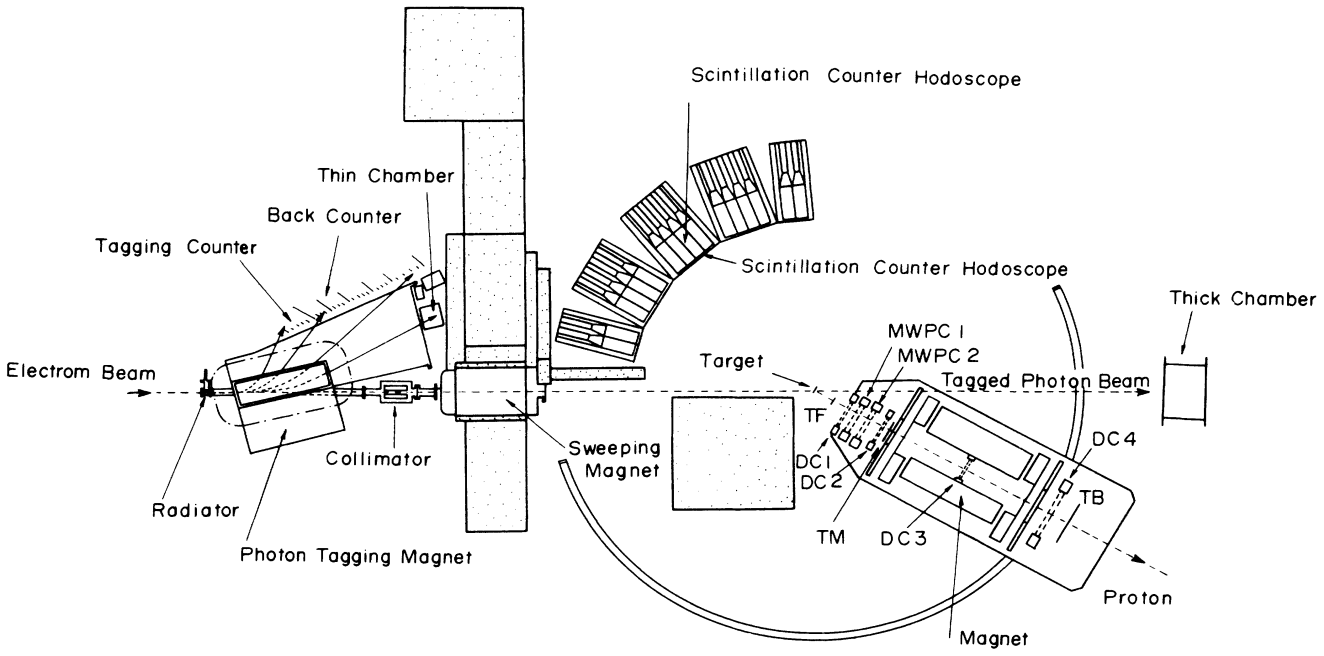

FIG. 1. Experimental apparatus.

mined was about 5% in the momentum region greater than 600 MeV/c. The angular acceptances of the spectrometer were about $\pm 5°$ horizontally and $\pm 7°$ vertically. The resultant solid angle of the spectrometer was about 33 msr in the momentum region greater than 400 MeV/c.

The separation of protons from positrons, pions, and deuterons was made by a measurement of the time of flight (TOF) between two triggering counters, TF and TB, in the spectrometer.

D. Hodoscope

The hodoscope consisting of 64 scintillation counters (each had the dimensions $150\times 150\times 300$ mm^3) was used to measure the momentum vector of the neutrons or protons accompanying the spectrometer protons. These hodoscope counters were placed 150 cm from the target and covered the angular range 90°—170° on the opposite side of the magnetic spectrometer. In front of the hodoscope, 16 scintillation counters were placed in order to separate charged particles from neutral particles. The momenta of the protons and neutrons were determined by the measurement of the time of flight between the TF counter in the spectrometer and the hodoscope. In Fig. 2 examples of the TOF spectrum and the TOF—pulse height plot are shown for the beryllium target run. For the events in which the spectrometer detected the protons and the hodoscope detected neutral particles, the photons from the decay of neutral pions in the reaction $\gamma + \text{"p"} \rightarrow \text{p} + \pi^0$, and the neutrons from the reaction $\gamma + \text{"pn"} \rightarrow \text{p} + \text{n}$, are clearly separated. The photons were identified as the events whose TOF values were between 0 and 10 ns, and the neutrons were identified as the events whose TOF values were between 10 and 25 ns. For the charged particle events in which the spectrometer detected protons and the hodoscope detected charge particles, the protons were not separated from the charged pions unambiguously by the TOF information only. Therefore, the pulse height information from the hodoscope was used in addition to the TOF information. In Fig. 2(b), a scatter plot of the pulse height and TOF is shown. In this figure, pions were identified as the events which lay between line 1 and line 2, and protons were identified as the events which lay between line 2 and line 3. The estimated probability of misidentifying pions as protons in this method was about 7% of proton events, and that of misidentifying protons as pions was 4% of proton events.

The resolution of this TOF measurement was ± 0.9 ns (FWHM), which corresponded to the momentum resolution of ± 20 MeV/c (FWHM) at 400 MeV/c for protons or neutrons. The threshold level of the hodoscope was set at 2 MeV for electrons. In this setting, the detection efficiency[12] for neutrons was calculated to be about (33 ± 1.6)% over the momentum greater than 400 MeV/c. To check the momentum and efficiency determinations for neutrons, the hodoscope system was calibrated using the neutrons from the reaction $\gamma + \text{d} \rightarrow \text{p} + \text{n}$, as shown in Fig. 3, where protons were detected by the magnetic spectrometer. The detection efficiency was checked within an error of ± 5%. The histograms are the Monte Carlo simulations using the parameters used in the analysis of the neutron data.

E. Electronics and on-line data acquisition system

The coincidence signals between the tagging counters and the corresponding backing counters were added together to give a signal of the tagged photon $[\text{TAG}=\Sigma(\text{T}_i\cdot\text{B})]$.

The threefold coincidence signal $\text{T}=\text{TF}\cdot\text{TM}\cdot\text{TB}$ defined the passage of a particle through the magnetic spectrometer.

The twofold coincidence signal T·TAG was used as a

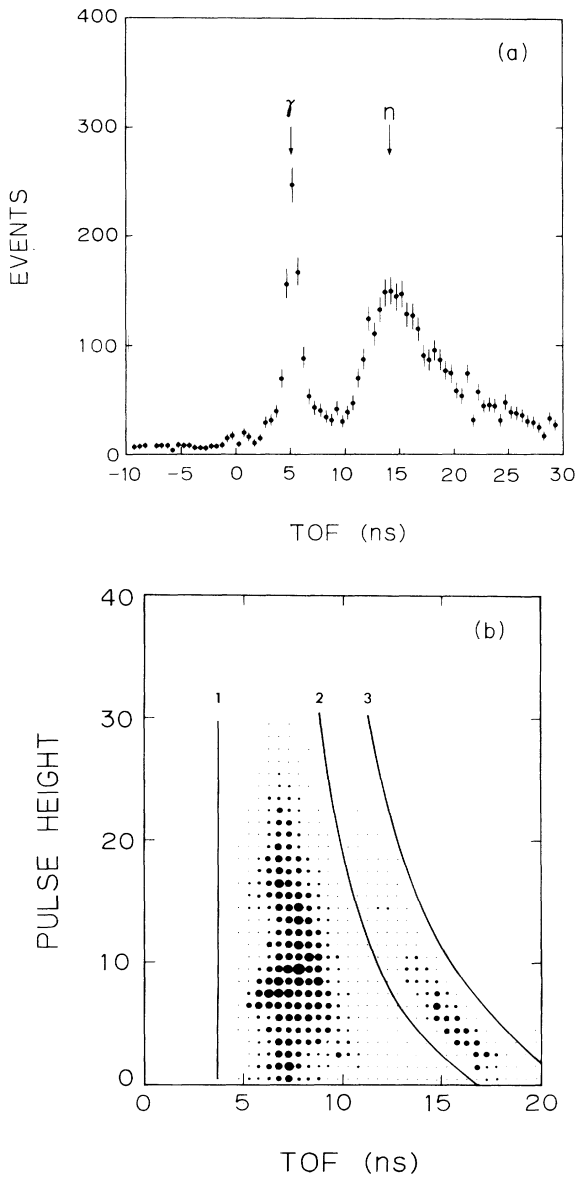

FIG. 2. (a) TOF spectra for the neutral particles detected by the hodoscope. (b) Scatter plot of TOF and pulse height for the charged particles.

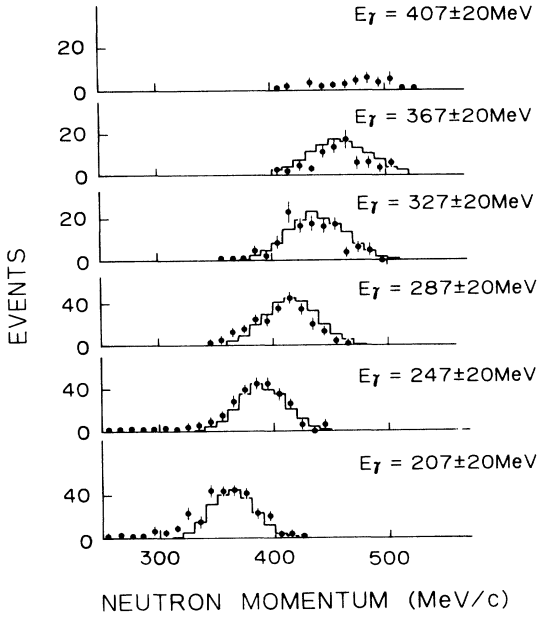

FIG. 3. The momentum spectra of neutrons detected by the hodoscopes in coincidence with the spectrometer protons in the reaction of $\gamma + d \rightarrow p + n$. The histograms are the results of a Monte Carlo simulation using the parameters used in the analysis of the hodoscope data.

master signal. The width of the coincidence of the master trigger was 17 ns. The master signal was used (1) as the gate pulse for the MWPC readout, (2) as the start pulse for time-to-digital convertors (TDC's), (3) as the gate pulse for analog-to-digital convertors (ADC's), (4) as the strobe signal for coincidence registers, and (5) as the start signal of the CAMAC data acquisition.

Data from the CAMAC modules were read into an on-line terminal computer, PANAFACOM-U400 event by event. This computer stored the raw data on disks and transferred them into a central computer, FACOM-M180, for on-line analyses of the data. Both the raw and analyzed data were stored in magnetic tapes at the central computer for later analyses.

III. DATA REDUCTION

A. Single-arm experiment

In each of the accumulated events, the particle trajectory was reconstructed using the coordinates measured by the chambers located upstream and downstream from the magnet in the spectrometer in order to determine the emission angle and the momentum of the protons. After this, the accepted events were grouped into a momentum bin width of 20 MeV/c. This bin width was chosen to be comparable to the momentum resolution of the spectrometer. The accepted events were also grouped into an incident energy bin of 20 MeV.

Various corrections were made on the raw data in the process of calculating the differential cross sections. The efficiency of the trajectory reconstruction was about 97%. Accidental coincidence was about 10% for T·TAG. The pion and deuteron contaminations in the proton events in the spectrometer were estimated at less than 1%. The counting rate without the target was less than 0.5% of the rate with the target after the cut in the reaction point was made. The empty target rate was about 2% for the liquid deuterium and water. The nuclear absorption corrections at the target and spectrometer were about 4% at 400 MeV/c and about 2% at momenta greater than 600 MeV/c.

After the above corrections were made on the raw data, the differential cross sections of the reactions,

$$\gamma + A \rightarrow p + \text{anything} \quad [A = {}^2H,\ {}^9Be,\ {}^{12}C, \text{ and } H_2O\ ({}^{16}O)], \tag{5}$$

were calculated from the proton yield Y_p by the following equation,

$$\frac{d^2\sigma}{dP_p d\Omega_p} = \frac{Y_p}{N_\gamma \cdot N_T \cdot \Delta P \cdot \Delta\Omega}\ , \tag{6}$$

where N_γ was the number of incident protons, N_T was the number of target nuclei per cm^2, ΔP was the momentum bin width, and $\Delta\Omega$ was the solid angle of the spectrometer. The solid angle of the spectrometer was calculated by a Monte Carlo method, which took account of the detector geometry, energy losses in the materials, the scattering in and out due to the multiple Coulomb effect, and the distribution of the magnetic field.

B. Coincidence experiments

In each of the proton events in the spectrometer, the hodoscope information was required in order to identify the reaction. Since the hodoscope can detect and identify the photons, pions, protons, and neutrons, the proton spectrum measured by the spectrometer was classified by the hodoscope information into (γ,pγ), (γ,pπ), (γ,pn), and (γ,pp) reactions, where γ, π, p, and n are detected by the hodoscope.

The momentum spectra of protons in the magnetic spectrometer, classified by the hodoscope information, are shown in Fig. 4 for ^{2}H, and ^{9}Be targets at the incident photon energy of 327 MeV. In this figure, the uppermost panels show the single-arm proton spectra for the reaction of (γ,p). Panels (A), (B), (C), and (D) show the spectra for the reactions (γ,pγ), (γ,pn), (γ,pπ), and (γ,pp), where γ, n, π, and p are detected by the hodoscope array.

For the deuterium target, the single-arm proton spectrum shows two peaks. The low-momentum peak (the first peak) corresponds to the reactions of the quasifree pion production,

$$\gamma + p + (n) \rightarrow p + \pi^0 + (n) \tag{7}$$

and

$$\gamma + n + (p) \rightarrow p + \pi^- + (p)\ , \tag{8}$$

where particles in parentheses are the spectator nucleons. The high-momentum peak (the second peak) corresponds to the photodisintegration reaction,

$$\gamma + d \rightarrow p + n\ . \tag{9}$$

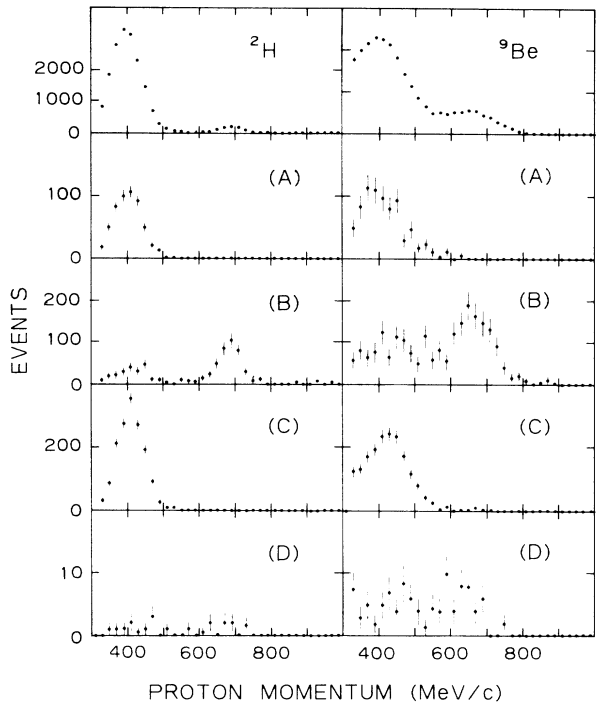

FIG. 4. Examples of the momentum spectra of protons for ^{2}H(γ,p) and ^{9}Be(γ,p) at the photon energy of 327 MeV with the requirements of (top) none, (a) γ's, (b) neutrons, (c) pions, and (d) protons in the hodoscope.

These reaction identifications were based on the fact that two peaks in the spectrum were located in the right positions expected from the kinematics of corresponding reactions. When we take the coincidence with the hodoscope signals, the second peak remains only in the (γ,pn) channel. A very small number of high momentum protons remain in the (γ,pp) channel. Proton yield in this high momentum region is about 3% of the neutron yield and can be explained by the misidentification of neutrons as protons. On the other hand, the first peak remains in all reaction channels. In the (γ,pγ) channel, the hodoscope detects the photons from the decay of neutral pions in reaction (7). In the (γ,pπ) channel, the hodoscope detects the charged pions in reaction (8). In the (γ,pn) channel, the hodoscope detects the spectator neutron in reaction (7) and in the (γ,pp) channel the hodoscope detects the spectator proton in reaction (8).

For the ^{9}Be target, almost the same features are obtained. The only difference is the enhanced proton yield in the (γ,pp) channel. The high momentum protons in the (γ,pp) channel for the deuterium target come only from the misidentification of neutrons. However, for ^{9}Be, the quasifree reaction,

$$\gamma + \text{“pp”} \rightarrow \text{p} + \text{p} \ , \tag{10}$$

can take place in addition to the quasifree reaction

$$\gamma + \text{“pn”} \rightarrow \text{p} + \text{n} \ , \tag{11}$$

and this yields the (γ,pp) events in the high momentum region. From these coincidence measurements, the quasifree reactions (10) and (11) were identified and separated from the backgrounds.

Angular correlations between the spectrometer proton and the hodoscope particle give us another confirmation on the reaction channel. Angular correlations for each reaction channel are shown in Fig. 5, where panels (a), (b), (c), and (d) show the results for the reaction channels (γ,pγ), (γ,pπ), (γ,pn), and (γ,pp), respectively.

In the deuterium target data, characteristic features of the angular correlation are clearly shown. For the (γ,pγ) and (γ,pπ) channels, events are peaked at the laboratory angle of 90°, which is expected from the kinematics of the quasifree pion production. For the (γ,pn) channel, events are clustered at the laboratory angle of 130°. The width of the peak is $\pm 10°$, which is expected from the angular acceptance of the magnetic spectrometer. For ^{9}Be, although these angular correlations are smeared out by the relatively large internal motion of nucleons or two-nucleon systems in the nucleus, the basic structures are the same as those for the deuterium target.

Figure 6 shows the momentum scatter plot of (γ,pn) events for ^{2}H and ^{9}Be targets. In the case of the ^{2}H target, coincidence events are clustered at the momenta expected from the kinematics of the reaction $\gamma + \text{d} \rightarrow \text{p} + \text{n}$. In the case of the ^{9}Be target, a cluster of events is also clearly seen at the higher momentum region, and the center of this cluster is located at the momentum similar to the case of ^{2}H target. These figures again confirm that the pn coincidence in the higher momentum region comes mainly from the quasifree reaction (11). The pn coincidence events scattered in the lower momentum region are interpreted as being due to the photoproduction of pion from a single nucleon in the nucleus (γ + “N” $\rightarrow$ p + “π”) followed by pion-nucleon interactions (“π” + “N” $\rightarrow \pi$ + n) in the nucleus.

Cross sections for the quasifree reaction (11) for ^{9}Be and ^{12}C were deduced from the coincidence data. In addition to the correction due to the neutron detection efficiency, the correction for the geometrical detection efficiency of the hodoscope should be taken into account, since the hodoscope does not cover all the angular range of the neutrons in coincidence with the spectrometer proton. To calculate the geometrical acceptance of the hodoscope, the knowledge of the pn angular correlation in the quasifree reaction (11) is necessary. For this purpose, we used the momentum distribution of the “pn” system discussed in Sec. V, which reproduced the experimental data well. The selection of coincidence events for the quasifree reaction (11) was carried out using the criteria

$$\begin{aligned} &P_{\text{p}} > 1.5E_\gamma + 50 \text{ MeV}/c \text{ for } ^9\text{Be} \\ &\quad \text{and } > 1.5E_\gamma + 30 \text{ MeV}/c \text{ for } ^{12}\text{C} \ , \\ &P_{\text{n}} > 200 \text{ MeV}/c \text{ for } ^9\text{Be and } ^{12}\text{C} \ , \\ &E^s_{\text{pn}} < 70 \text{ MeV for } ^9\text{Be and } < 80 \text{ MeV for } ^{12}\text{C} \ , \end{aligned} \tag{12}$$

where E_γ is the photon energy, P_{p} is the momentum of the protons, P_{n} is the momentum of neutrons, and E^s_{pn} is the separation energy of pn systems in the nucleus discussed in Sec. V. These events selections were made so as

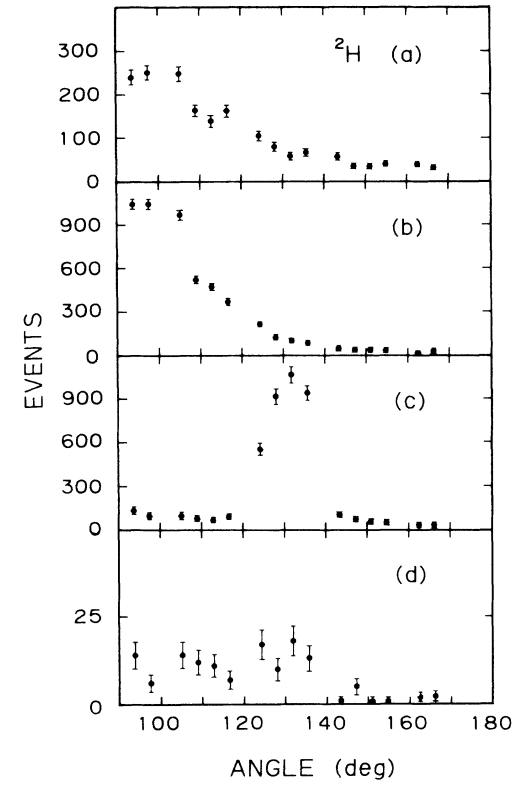

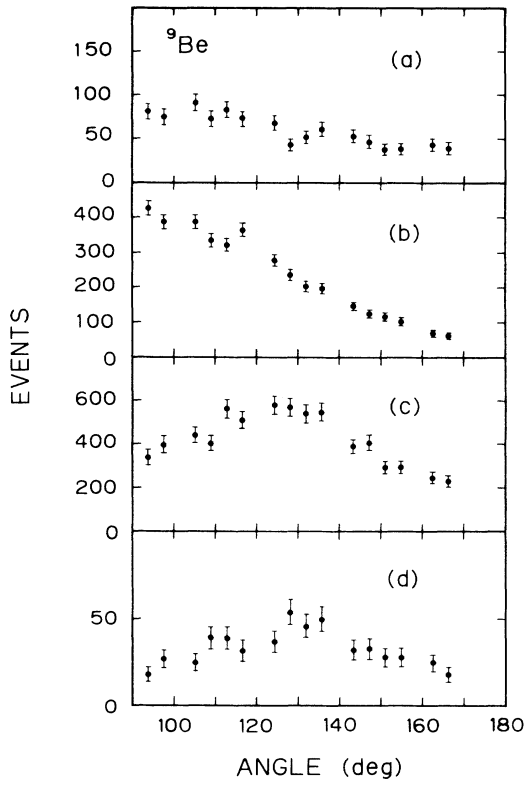

FIG. 5. Examples of the angular distributions of (a) γ's, (b) pions, (c) neutrons, and (d) protons, detected by the hodoscope in coincidence with the spectrometer protons at 30°.

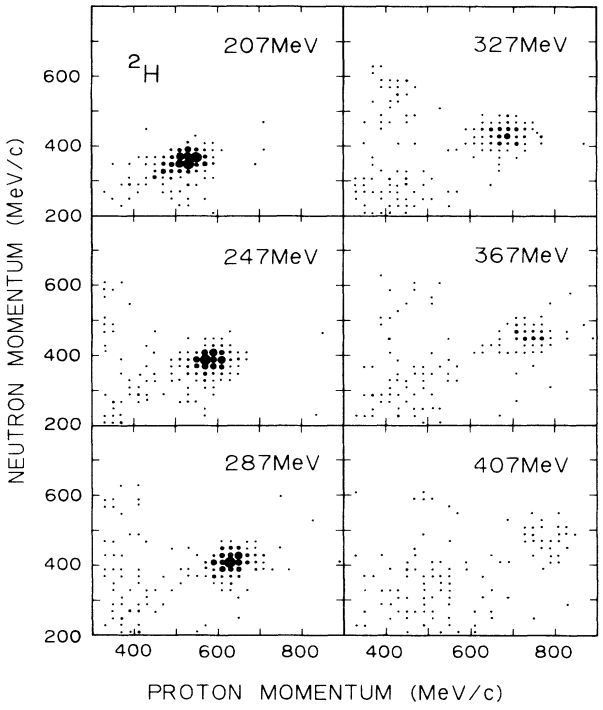

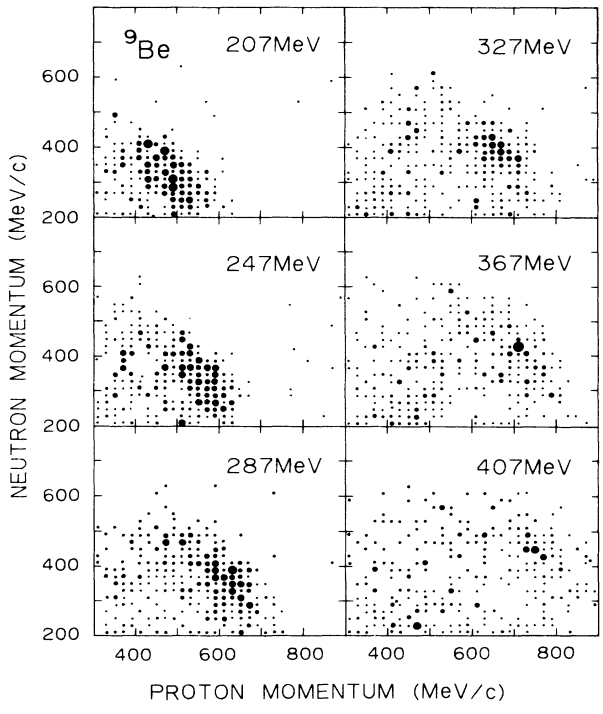

FIG. 6. The examples of the scatter plots of the momenta of protons and neutrons for ^{2}H and ^{9}Be.

TABLE I. Systematic errors (in percent) of cross sections for the reaction (γ,p) and (γ,pn).

Source of errors	^2H	^9Be	^{12}C	H_2O
(a) Number of photons	3	5	3	3
(b) Number of target nuclei	1	1	1	3
(c) Solid angle	3	3	3	3
(d) Reconstruction efficiency	2	2	2	2
(e) Empty target yield	3	1	1	2
(f) Accidental coincidence	2	2	2	2
(g) Nuclear absorption	1	1	1	1
(h) Proton identification	1	1	1	1
Quadratic sum for (γ,p)	6	7	5	6
(i) Neutron detection	5	5	5	5
(j) Neutron identification	3	3	3	3
(k) Neutron geometrical efficiency		5	5	5
Quadratic sum for (γ,pn)	8	10	9	10

to exclude only backgrounds and lose none of the true events.

IV. RESULTS

A. Single-arm experiments

The momentum spectra of protons from reaction (5) are shown in Fig. 7 for various targets at the incident energy of 357 MeV. The errors attached to the values of the cross sections are only statistical ones. The systematic errors are listed in Table I. A complete tabulation of the numerical values[13] of the cross sections is available from the Physics Auxiliary Publication Service (PAPS) depository.[14]

The momentum spectra obtained have the same shape as those in the previous paper[7] for ^9Be and ^{12}C; namely, two broad peak structures whose positions move as a function of incident energy. From the reasons discussed in Sec. III, the protons in these peaks are considered to come mainly from the quasifree two-body reactions (1) and (2). Therefore, the analysis of the momentum spectrum was performed by use of two Gaussian distributions corresponding to the quasifree two-body reactions (1) and (2) for ^2H, ^9Be, and ^{12}C. For the H_2O target, three Gaussian distributions were used, since the extra peak due to the photoproduction of pion from the free proton contributes to the spectrum.

Results of the fitting in this analysis are shown in Fig. 7 by solid curves. Two Gaussian functions for ^2H, ^9Be, and ^{12}C, and three Gaussian functions for the H_2O target, are shown separately. Overall features of the proton spectra are well reproduced.

The positions of the first peaks for ^2H, ^9Be, and ^{12}C are shown in Fig. 8 as a function of the photon energy. The positions of the peaks expected from the reaction $\gamma+p\rightarrow p+\pi^0$ are also shown by the solid line in the figure. The peak positions for nucleus targets shift to the lower momentum side from those expected from the free proton reaction. The amount of the shift was 10—20 MeV/c for $^2H(\gamma,p)$ and 20—40 MeV/c for $^9Be(\gamma,p)$ and $^{12}C(\gamma,p)$, and depends on the photon energy. These shifts are interpreted as being due to the nuclear binding effect of target nucleons "N" in the nucleus. Positions of the second peaks for ^2H, ^9Be, ^{12}C, and ^{16}O are shown in Fig. 9. The calculated positions expected from the free deuteron reaction $\gamma+d\rightarrow p+n$ are shown by the solid line, where we can see that the results from the deuterium target are in good agreement with the calculated ones. It is noted that the amount of shift does not depend on the photon energy and is about 35 MeV/c for $^9Be(\gamma,p)$ and 40 MeV/c for $^{12}C(\gamma,p)$ and $^{16}O(\gamma,p)$. These values are about 2 times larger than the shift of the first peak. The results

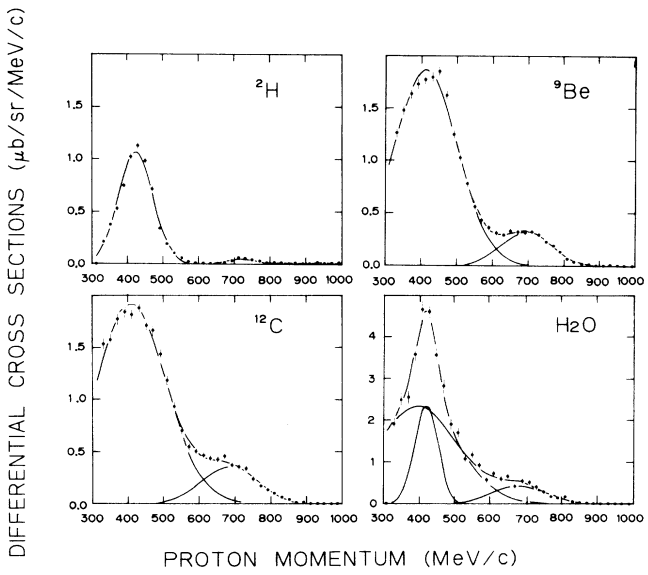

FIG. 7. The momentum spectrum of photoemitted protons detected at 30° and at the photon energy of 375 MeV for various target nuclei.

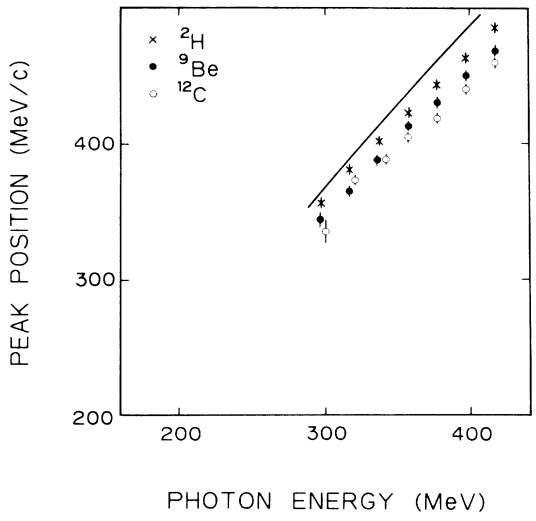

FIG. 8. The position of the first peak in the momentum spectrum of protons as a function of the photon energy for ^{2}H, ^{9}Be, and ^{12}C. The solid line is a calculated position expected from the reaction $\gamma + p \rightarrow p + \pi^0$.

are understood quite naturally as nuclear binding effects; the single nucleon "N" participates in the first peak, and two nucleons "pN" participate in the second peak.

The cross sections of the reaction $\gamma + p \rightarrow p + \pi^0$ were deduced from the proton spectra for the water target and those of the reaction $\gamma + d \rightarrow p + n$ were obtained from the proton spectra for the liquid deuterium target. Results of these cross sections are shown in Figs. 10 and 11 in the center-of-mass system. For comparison, recent data[15] from the Bonn synchrotron are shown. Present results are in reasonable agreement with those data.

The differential cross sections for individual quasifree reactions (1) and (2) were obtained by integrating the Gaussian functions over the momentum and are shown in Fig. 12 and Fig. 13. Numerical results are listed in Table II. Errors are statistical only.

The photon energy dependence of the cross sections for the reaction $\gamma + p \rightarrow p + \pi^0$ shows a broad peak at the photon energy of 330 MeV, and that for $\gamma + d \rightarrow p + n$ also shows the broad peak at around 270 MeV. These peaks are considered to be due to the excitation of the $\Delta(1232)$ resonance. For nuclear targets, enhancements of the cross sections for both quasifree reactions are also observed in this energy region, indicating that the contribution of the $\Delta(1232)$ resonance is also important in these reactions.

The photon energy dependence of the cross sections differs slightly in each quasifree reaction and for each target nucleus. For the quasifree pion production, the photon energy which gives the maximum cross section becomes higher as the target mass number increases. This is considered to be due to the effect of the final state interactions of the recoil protons. For the photodisintegration of the two-nucleon system, the shape of the photon energy dependence of the cross sections does not change so much for all nucleus targets investigated. This implies that the mechanism of the photodisintegration of the two-nucleon system in the nucleus is very close to that of free deuteron. The difference in the maximum position of the Δ resonance of the two quasifree reactions may be due to the binding effects of the target nucleon or two-nucleon systems in the nucleus.

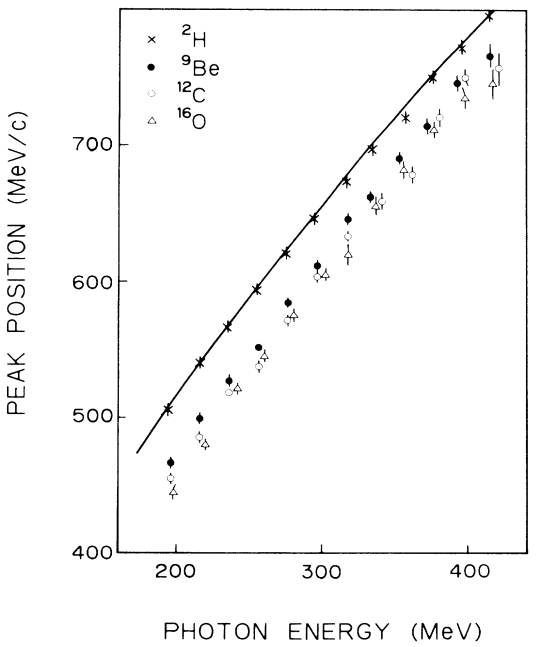

FIG. 9. The position of the second peak in the momentum spectrum of protons as a function of the photon energy for ^{2}H, ^{9}Be, ^{12}C, and ^{16}O. The solid line is a calculated position expected from the reaction $\gamma + d \rightarrow p + n$.

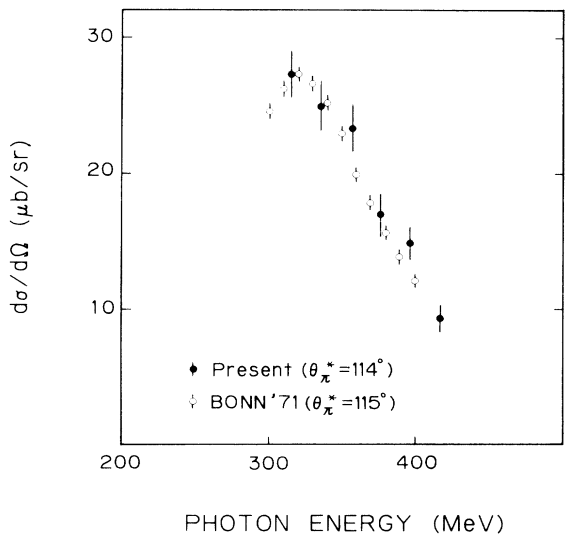

FIG. 10. The cross sections of the reaction $\gamma + p \rightarrow p + \pi^0$ as a function of the photon energy. The present results are deduced from the proton spectra for the water target.

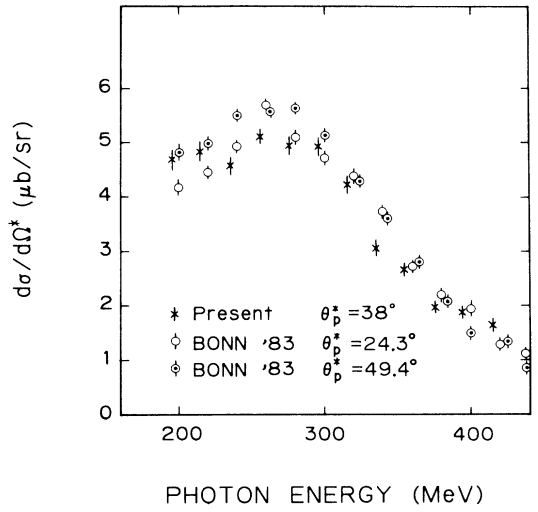

FIG. 11. The cross sections of the reaction $\gamma + d \rightarrow p + n$ as a function of the photon energy.

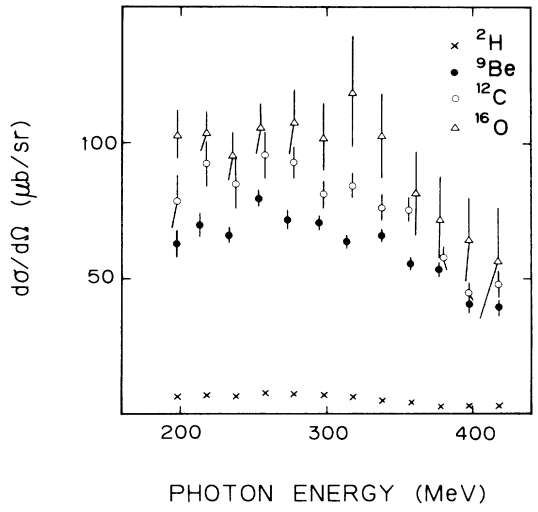

FIG. 13. The cross sections of the reaction $\gamma +$ "pN" $\rightarrow p + N$ as a function of the photon energy for various target nuclei.

B. Coincidence experiments

The numerical values of cross sections for reaction (11) obtained by the coincidence experiment are listed in Table III and are plotted in Fig. 14 for ^{9}Be and ^{12}C as a function of the photon energy. In this case the cross sections are obtained with a photon energy bin of 40 MeV. The energy dependence of the cross sections exhibits behavior similar to that derived from the single-arm data. However, absolute cross sections are about 40% of the cross sections derived from the single-arm data, in which the contribution of the quasifree reaction (10) is included.

The ratios of the cross sections between reactions (10) and (11) were obtained from the coincidence experiments. The results are shown in Fig. 15 and listed in Table V for ^{9}Be and ^{12}C as a function of the incident photon energy.

Table IV shows the ratio of cross sections for reaction (11) derived from the proton-inclusive data and those from the pn coincidence data. In this analysis, contribution from reaction (10) is subtracted from the inclusive data. This ratio shows directly the probability that the neutron in the quasifree reaction (11) leaves the nucleus without interaction with the rest of the nucleus. The averaged values of this probability in the present energy region are 0.50 ± 0.08 for ^{9}Be and 0.39 ± 0.12 for ^{12}C.

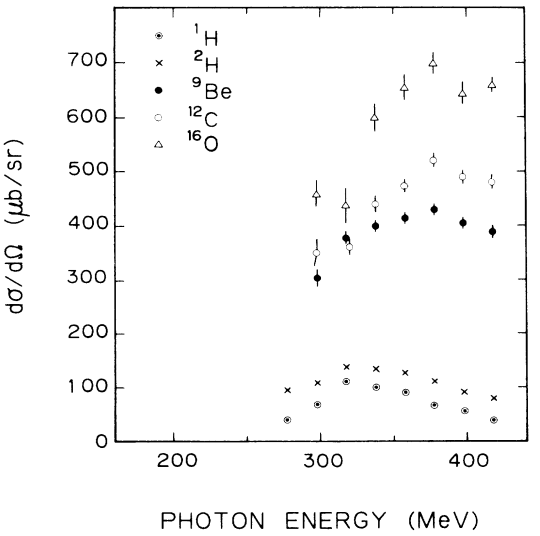

FIG. 12. The cross sections of the reaction $\gamma +$ "N" $\rightarrow p + \pi$ as a function of the photon energy for various target nuclei.

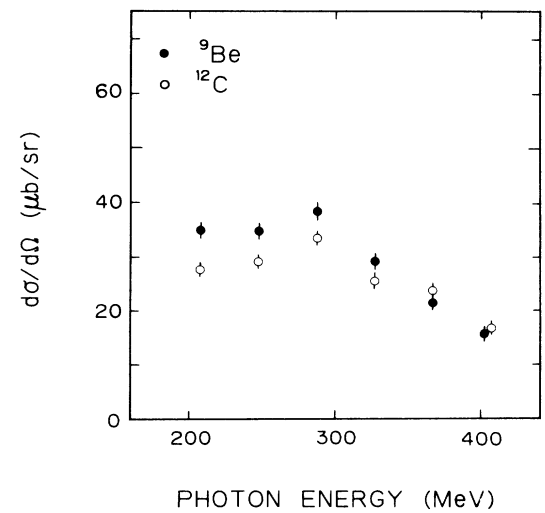

FIG. 14. The cross sections of the reaction $\gamma +$ "pn" $\rightarrow p + n$ obtained by the pn coincidence measurement as a function of the photon energy for ^{9}Be and ^{12}C.

TABLE II. Differential cross sections for the quasifree reactions γ + "N"$\rightarrow\pi$ + p and γ + "pN"$\rightarrow$p + n at the proton laboratory angle of 30°±4°.

Photon energy (MeV)	γ + d$\rightarrow$p + anything $d\sigma/d\Omega$ [reaction (1)] (μb/sr)	$d\sigma/d\Omega$ (γd$\rightarrow$pn) (μb/sr)	Photon energy (MeV)	$\gamma+{}^{12}$C$\rightarrow$p + anything $d\sigma/d\Omega$ [reaction (1)] (μb/sr)	$d\sigma/d\Omega$ [reaction (2)] (μb/sr)
197±10		6.70±0.26	197±10		78.6±9.5
217±10		7.08±0.28	217±10		92.5±8.4
237±10		6.76±0.28	237±10		85.5±9.6
257±10		7.73±0.30	257±10		96.0±8.5
277±10	96.5±6.2	7.51±0.30	277±10		93.5±6.5
297±10	109.0±2.3	7.54±0.32	297±10	350.5±33.5	81.6±5.6
317±10	138.2±1.8	6.71±0.32	317±10	467.7±14.8	84.5±4.3
337±10	135.3±1.5	4.94±0.27	337±10	440.6±13.7	76.6±4.5
357±10	128.8±1.4	4.40±0.26	357±10	474.5±11.7	75.8±4.9
377±10	113.3±1.3	3.27±0.22	377±10	521.3±11.5	57.9±5.2
397±10	93.6±1.2	3.18±0.23	397±10	490.7±8.5	45.2±3.8
417±10	80.2±1.1	2.81±0.21	417±10	481.5±7.7	48.2±6.3
Photon energy (MeV)	$\gamma+{}^{9}$Be$\rightarrow$p + anything $d\sigma/d\Omega$ [reaction (1)] (μb/sr)	$d\sigma/d\Omega$ [reaction (2)] (μb/sr)	Photon energy (MeV)	$\gamma+{}^{16}$O$\rightarrow$p + anything $d\sigma/d\Omega$ [reaction (1)] (μb/sr)	$d\sigma/d\Omega$ [reaction (2)] (μb/sr)
197±10		62.8±4.7	197±10		102.9±8.9
217±10		70.2±4.8	217±10		104.4±7.5
237±10		66.7±2.7	237±10		95.6±9.0
257±10		79.9±3.0	257±10		106.0±9.3
277±10		72.2±2.7	277±10		108.9±12.6
297±10	305.6±16.9	71.3±2.3	297±10	459.7±24.3	102.3±13.0
317±10	377.1±13.4	64.4±2.4	317±10	439.3±33.7	118.9±20.5
337±10	399.5±8.7	66.2±2.4	337±10	603.9±27.5	103.5±16.8
357±10	415.6±6.8	56.7±2.4	357±10	657.7±23.9	81.6±16.5
377±10	432.3±6.6	53.9±2.9	377±10	699.4±20.9	72.3±16.5
397±10	404.4±5.6	41.4±2.3	397±10	642.1±18.9	64.5±15.3
417±10	391.6±5.4	39.6±3.1	417±10	662.4±17.8	56.5±21.7

V. DISCUSSION

A. Mass-number dependence of cross sections for quasifree reactions

The mass-number dependences of the cross sections for the quasifree reactions (1) and (2) were obtained from the single-arm data, where the cross sections were averaged over the photon energy region from 297 to 417 MeV for reaction (1), and from 197 to 417 MeV for reaction (2). The results are shown in Fig. 16. When the data on ^{9}Be, ^{12}C, and ^{16}O are fitted with the form

$$\frac{d\sigma}{d\Omega}(A)=aA^{b}, \tag{13}$$

b values of 0.70±0.03 for reaction (1) and 0.71±0.06 for reaction (2) are obtained.

In this $\Delta(1232)$ resonance region, photons are absorbed

TABLE III. Cross sections for the quasifree reaction γ + "pn"$\rightarrow$p + n obtained from the proton-neutron coincidence data.

Photon energy (MeV)	^{9}Be (μb/sr)	^{12}C (μb/sr)
207±20	35.0±1.3	28.1±1.2
247±20	35.1±1.3	29.4±1.3
287±20	38.4±1.4	33.8±1.4
327±20	29.6±1.3	25.9±1.3
367±20	22.0±1.2	24.1±1.3
407±20	16.4±1.1	17.0±1.1

TABLE IV. Ratios of cross sections for the quasifree reaction γ + "pp"$\rightarrow$p + p to those for the quasifree reaction γ + "pn"$\rightarrow$p + n.

Photon energy (MeV)	^{9}Be	^{12}C
207±20	0.062±0.020	0.111±0.032
247±20	0.070±0.018	0.115±0.025
287±20	0.031±0.012	0.092±0.021
327±20	0.083±0.020	0.120±0.028
367±20	0.078±0.022	0.081±0.024
407±20	0.061±0.023	0.097±0.031

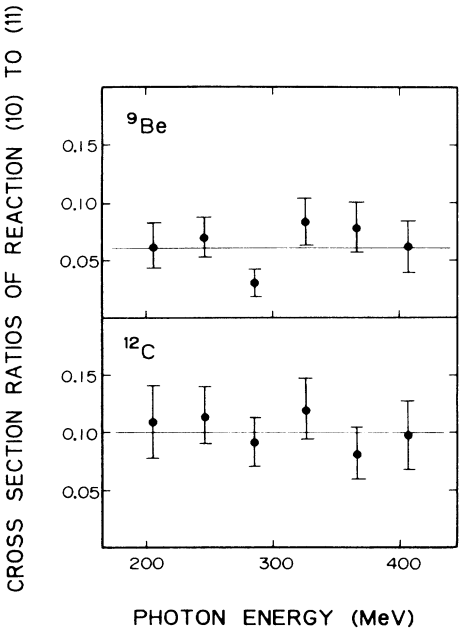

FIG. 15. The ratios of the cross sections of the reaction γ + "pp"→p + p to the reaction γ + "pn"→p + n as a function of the photon energy for ^{9}Be and ^{12}C.

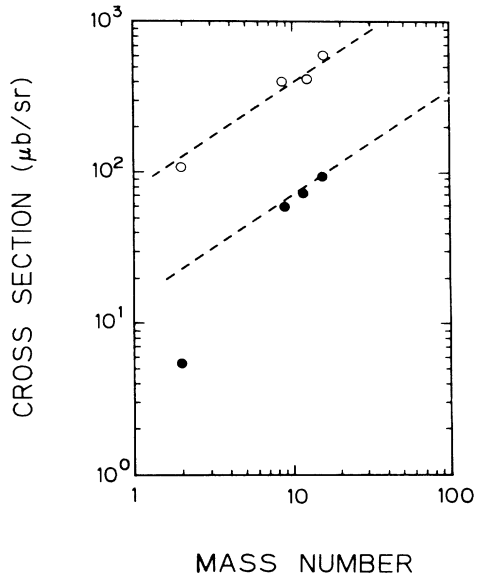

FIG. 16. The mass number dependence of the average cross sections of the reactions γ + "N"→p + π and γ + "pN" →p + N. The dashed lines indicate $A^{0.70}$ and $A^{0.71}$ dependence.

mainly through two quasifree reactions, (1) and (2). For reaction (1), since the nuclear shadowing effect for the incident photon is negligible, the cross section is considered to be proportional to A, if the final state interaction of outgoing protons is neglected. The present result, however, shows that the cross section is proportional to $A^{2/3}$. This suggests that, although the quasifree reaction takes place in proportion to A in the nucleus, a part of protons suffered the final state interaction in the nucleus.

The mass-number dependence of cross sections for the quasifree reaction (2) shows A dependence similar to that of reaction (1) in the mass number range $9 \leqq A \leqq 16$. Since the cross section of the proton-nucleon interaction in the proton momentum range for reaction (1) and that for reaction (2) does not change strongly, the attenuation due to the final state interaction for both reactions can be considered to be the same. This means that the A dependence of reaction (2) is also proportional to A.

Information on final state interactions of nucleons in the nucleus can also be obtained from the coincidence data. The cross sections of reaction (2) deduced from the coincidence data, and those from the proton-inclusive data, must be the same, if the neutrons do not suffer from the final state interactions. Experimental values of the ratios of the cross sections are 0.5±0.08 for ^{9}Be and 0.39±0.12 for ^{12}C. Therefore, about 50% of the neutrons are considered to be scattered out from the quasifree region due to the final state interactions.

TABLE V. Ratios of cross sections for the quasifree reaction γ + "pn"→p + n obtained from the proton-neutron coincidence data to those obtained from the proton inclusive data.

Photon energy (MeV)	^{9}Be	^{12}C
207±20	0.56±0.04	0.37±0.03
247±20	0.51±0.03	0.37±0.03
287±20	0.55±0.03	0.43±0.03
327±20	0.49±0.03	0.37±0.03
367±20	0.43±0.03	0.39±0.03
407±20	0.43±0.04	0.40±0.04

B. Separation energy and momentum distributions of the two-nucleon system in the nucleus

In the present experiment the momentum vectors of the incident photon, the forward proton, and the backward proton or neutron were also measured. Therefore the separation energy of the two nucleon system from the nucleus and the momentum of the two nucleon system in the nucleus can be calculated event by event.

The momentum and energy conservations for the reaction

$$\gamma + \mathrm{A} \rightarrow \mathrm{p} + \mathrm{N} + \mathrm{X} \quad (\mathrm{N} = \mathrm{p} \text{ or } \mathrm{n}) \tag{14}$$

are written as follows,

$$k = P_\mathrm{p} + P_\mathrm{N} + P_\mathrm{X} , \tag{15}$$

$$E_\gamma + M_\mathrm{A} = E_\mathrm{p} + E_\mathrm{N} + E_\mathrm{X} , \tag{16}$$

where (E_γ, k), $(E_\mathrm{p}, P_\mathrm{p})$, and $(E_\mathrm{N}, P_\mathrm{N})$ denote the four-momenta of the incident photon, the proton, and the other proton or neutron in the final state, respectively. The

four-momentum (E_X,P_X) of the undetected $(A-2)$ nucleon system X is obtained by use of the above equations. Consequently, the invariant mass M_X of the $(A-2)$ system is determined by an equation,

$$M_X^2=E_X^2-P_X^2 . \quad (17)$$

Further, we define a separation energy E_{pn}^s by the equation

$$E_{pn}^s=(M_X+M_p+M_N)-M_A , \quad (18)$$

where M_p, M_N, and M_A are the mass of proton, proton or neutron, and target nucleus, respectively.

For the quasifree reaction (2), the momentum of the two-nucleon system in the nucleus P_{pN} was calculated by the impulse approximation as follows,

$$P_{pN}=P_p+P_N-k . \quad (19)$$

The calculation of the separation energy and the momentum distribution of the two-nucleon system in the nucleus was also applied to the deuteron target data for the check of the above procedure.

Examples of measured distributions of the separation energy E_{pn}^s for ^{2}H, ^{9}Be, and ^{12}C are shown in Fig. 17 for the proton-neutron coincidence data at the incident photon energy of 287±20 MeV.

For the reaction $\gamma+d\rightarrow p+n$, since there is no missing particle in this process, E_{pn}^s should be centered around 2.2 MeV, the binding energy of the deuteron. The width of the distribution shows the instrumental resolution of the present detection system. The measured resolution is about 30 MeV in this energy region. In the case of ^{9}Be(γ,pn) and ^{12}C(γ,pn), the peaks located at about 35 MeV for ^{9}Be and about 45 MeV for ^{12}C are obtained. In addition to the main peak, the broad bumps are seen at the higher separation energy. These are considered to come from the pion production in the final state.

For the proton-proton coincidence data, the distributions of the separation energy E_{pp}^s are shown in Fig. 18. The peak structures are not as clear as the ones in the reaction (γ,pn).

The examples of the momentum distributions of proton-neutron system in the nucleus are shown in Fig. 19 for ^{2}H, ^{8}Be, and ^{12}C at the photon energy of 287±30 MeV. In this analysis the events in the proton and neutron momentum regions corresponding to the quasifree reaction (11) were selected using the restriction (12). For the photodisintegration of the deuteron, the target deuterons are at rest, so that the momentum distribution has a peak at the momentum close to 0 MeV/c. The width of the distribution is due to the resolution of the present detection system. The results for the reactions ^{9}Be(γ,pn) and ^{12}C(γ,pn), whose peaks are located at 120—130

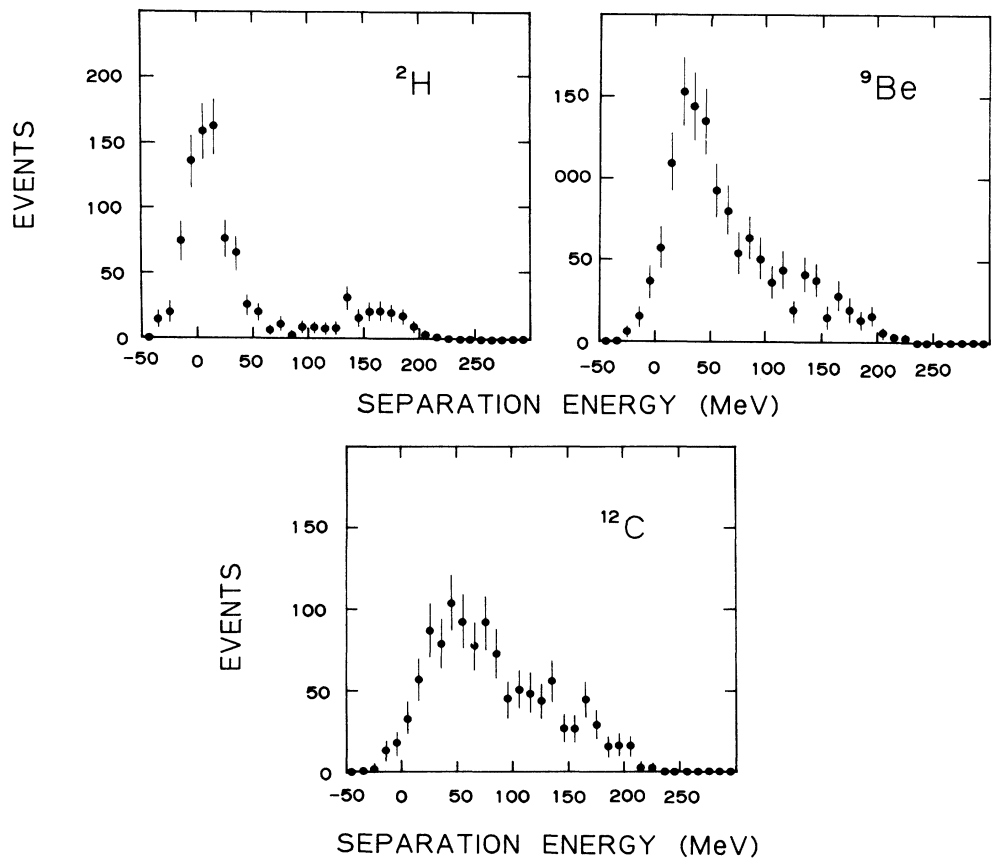

FIG. 17. Examples of the separation energy distributions E_{pn}^s for ^{2}H, ^{9}Be, and ^{12}C at the photon energy of 287 MeV.

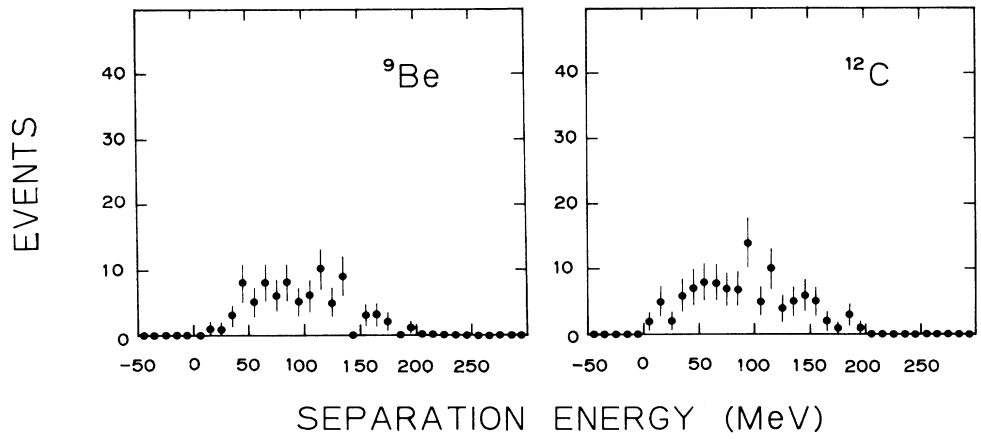

FIG. 18. Examples of the separation energy distributions E_{pp}^{s} for ^{9}Be and ^{17}C at the photon energy of 287 MeV.

MeV/c, have a much broader distribution.

The measured distributions of the separation energy and the momentum were analyzed with a Monte Carlo calculation[16] based on the independent particle model with a harmonic oscillator potential for the nuclear wave function.

Results of the calculation on the separation energies for ^{9}Be and ^{12}C are shown in Fig. 20 by a histogram, together with the experimental data at the photon energies of 247±60 MeV, where the parameter σ (harmonic oscillator parameter) is taken to be 80 MeV/c. This parameter was not sensitive to the results on the separation energy. The calculated distribution reproduced the experimental data reasonably well. However, the peak position is shifted toward higher energy by 10 MeV for both ^{9}Be and ^{12}C.

A typical example of the momentum distribution for

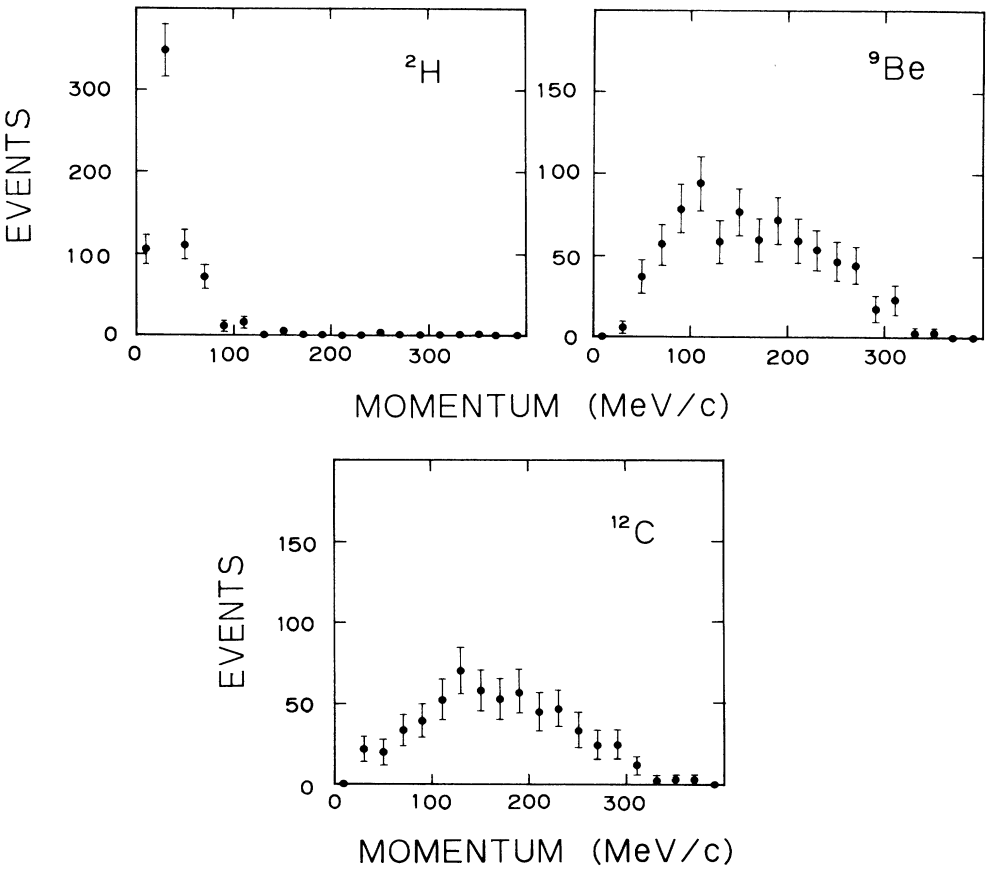

FIG. 19. Examples of the momentum distributions of pn systems in the ^{2}H, ^{9}Be, and ^{12}C at the photon energy of 287 MeV.

p-n events from ^{9}Be and ^{12}C at photon energies of 247±60 MeV is shown in Fig. 21. The momentum distribution is also analyzed by a Monte Carlo calculation,[16] where the harmonic oscillator parameter σ is the only free parameter. The results on the momentum distribution are well reproduced by a calculation with $\sigma=80$ MeV/c in both cases of ^{9}Be and ^{12}C, as shown in Fig. 21. With the same calculation, angular correlations between the proton and the neutron were obtained. Experimental results are reproduced with $\sigma=80$ MeV/c for ^{9}Be, as shown in Fig. 22. From these analyses, it can be concluded that each nucleon participating in the photodisintegration reaction has the momentum distribution with $\sigma=80$ MeV/c. It should be noted that the result of the calculation is not affected seriously by a choice of separation energies.

A similar Monte Carlo calculation was made to simulate the first peak. A result for ^{9}Be is illustrated in Fig. 23, together with the experimental data. The proton inclusive momentum spectrum in the first peak region is well reproduced by a calculation with $\sigma=120$ MeV/c. This value is consistent with the result obtained from other experiments on the reactions (e,e'p) and (p,2p).[17] Therefore there is a distinct difference between the σ values obtained from the quasifree reaction γ + "N" → p + π and the quasifree reaction γ + "pN" → p + N; namely, $\sigma=120$ MeV/c from the former reaction and $\sigma=80$ MeV/c from the latter reaction. This difference may indicate the possibility that the "pN" system in the nucleus

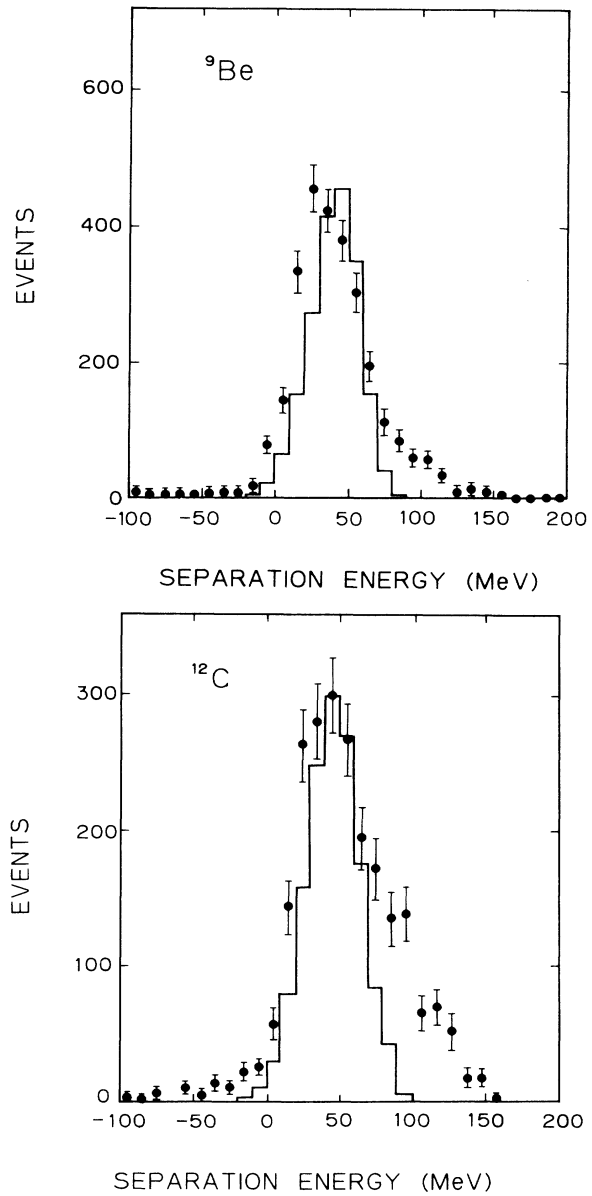

FIG. 20. The measured separation energy distribution at the photon energy of 247 MeV for ^{9}Be and ^{12}C. The histograms show the result of a Monte Carlo calculation based on the independent particle model with the harmonic oscillator parameter σ of 80 MeV/c.

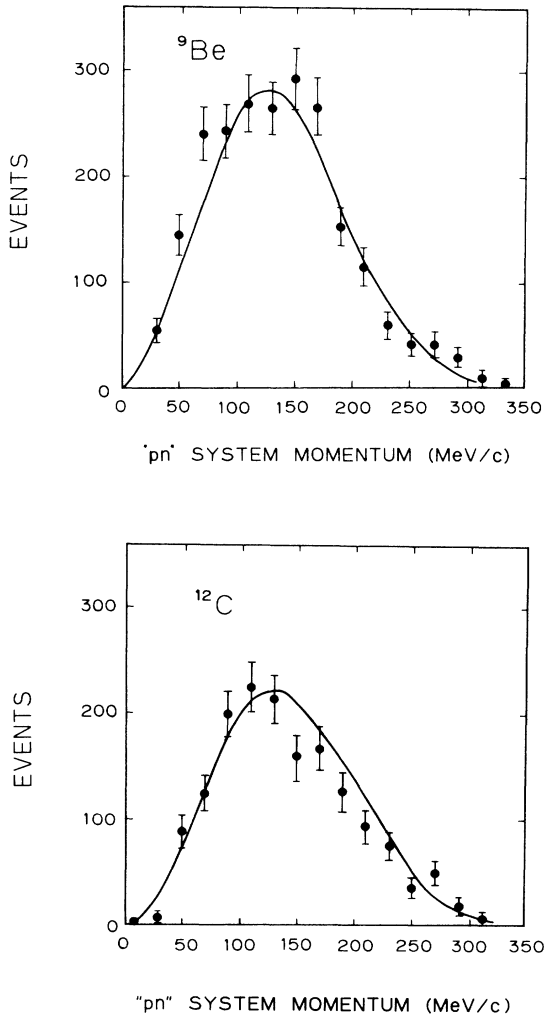

FIG. 21. The measured momentum distribution of pn systems in ^{9}Be and ^{12}C nuclei at the photon energy of 247 MeV. The solid curves show the results of a Monte Carlo calculation based on the independent particle model with the harmonic oscillator parameter σ of 80 MeV/c.

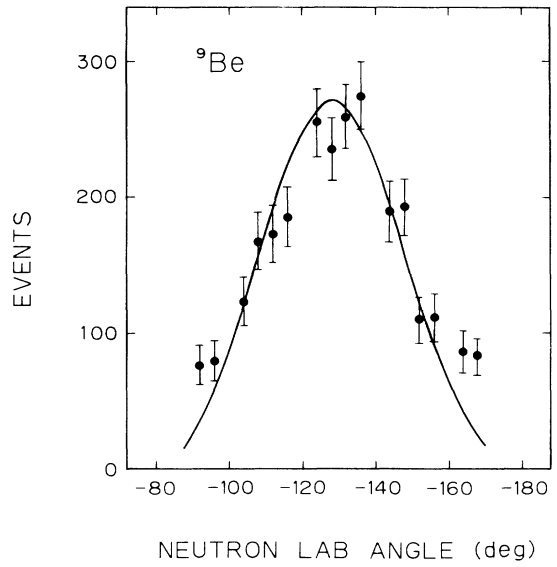

FIG. 22. The angular distribution of the neutrons in the reaction ^{9}Be(γ,pn) at the photon energy of 247 MeV and at the proton angle of 30°±4°. The solid curve is the result of a Monte Carlo calculation based on the independent particle model with the harmonic oscillator parameter σ of 80 MeV/c.

is not formed by a simple combination of two independent nucleons.

C. Comparison of cross sections for the quasifree reaction γ + "pN"→p + N with model analyses

Recently, model calculations of the cross section for the quasifree reaction γ + "pN"→p + N have been made by various authors[18–20] in the Δ(1232) resonance region. In these calculations, a diagram of the Δ(1232) formation was taken into account, together with some other diagrams. The results of the calculation reproduced the characteristic feature of the broad peak around the photon energy of 280 MeV. In addition to this photon energy dependence of cross sections, Wakamatsu and Matsumoto[18] and Homma and Tezuka[19] calculated cross sections for reactions (10) and (11) separately. Their results explained well the cross section ratio of the above two reactions.

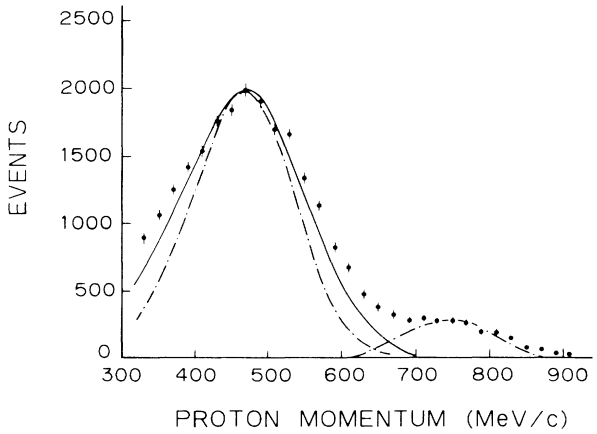

FIG. 23. The fitting of the momentum spectrum of the protons from the reaction of γ + ^{9}Be→p + anything at the photon energy of 407 MeV. The curves are the results of a Monte Carlo calculation based on the independent particle model with the harmonic oscillator parameters σ of 80 MeV/c (dashed-dotted line) and 120 MeV/c (solid line).

Wakamatsu and Matsumoto[18] calculated cross sections of both reactions (1) and (2) by use of the Fermi gas model for a nucleon in the nucleus. They used $U=40$ MeV for a depth of the one-body potential, and $P_F=195$ MeV/c for Fermi momenta on ^{9}Be and $P_F=221$ MeV/c for ^{12}C. Their calculation can explain the gross feature of the photon energy dependence of the cross section of reaction (2), where the cross section was maximum due to the Δ(1232) resonance.

Homma and Tezuka[19] studied the effect of the nuclear wave function in the cross section of reaction (2) by using three different types of two-nucleon wave functions: (1) the harmonic oscillator wave functions (the simple independent particle model) to form the two-nucleon system, (2) the Hulthén-type wave functions for two-nucleon systems, and (3) modified Hulthén-type wave functions. A favorable wave function for reproducing the data for ^{9}Be was obtained by shrinking the free-deuteron wave function to short distances. This may suggest the strong correlation between two nucleons participating in reaction (2).

Suzumura and Futami[20] also calculated the cross sections of reaction (11) by use of the Hulthén-type wave function for two-nucleon systems in the nucleus. In their calculation, ρ-meson-exchange diagrams were added to the diagrams used by Wakamatsu and Matsumoto. Varying the ρNN coupling constant within a permitted range, they can also explain the photon energy dependence of the cross section, which has its maximum around $E_\gamma=280$ MeV.

In these microscopic analyses of the photodisintegration reaction of the quasifree two-nucleon systems, cross sections for reactions (10) and (11) can be calculated separately. Wakamatsu and Matsumoto calculated the cross section ratio of reaction (10) to reaction (11) based on the Fermi gas model and obtained the value of $R=0.1$. On the other hand, Homma and Tezuka obtained $R=0.15$ for ^{9}Be. The smallness of this ratio is due to the ratio of the number of "pp" pairs to "pn" pairs in the nucleus (around 0.5) and the isospin characteristics of these reactions.

ACKNOWLEDGMENTS

The authors wish to thank Dr. K. Maruyama for his excellent advice in the design of this experiment and Dr. H. Tezuka for his helpful discussions on the experimental results. Thanks are also due the operating crew of the 1.3 GeV electron synchrotron, Institute for Nuclear Study, University of Tokyo, for their aid in the present experiment. This experiment was done by use of an on-line computer system at the Institute for Nuclear Study Computer Center.

[1]J. S. Levinger, Phys. Rev. **84**, 43 (1951).
[2]M. Q. Barton and J. H. Smith, Phys. Rev. **95**, 573 (1954); **110**, 1143 (1958).
[3]J. Garvey, B. H. Patrick, J. G. Rutherglen, and I. L. Smith, Nucl. Phys. **70**, 241 (1965); I. L. Smith, J. Garvey, J. G. Rutherglen, and G. R. Brookes, *ibid.* **B1**, 483 (1967).
[4]P. C. Stein, A. C. Odian, A. Wattenberg, and R. Weinstein, Phys. Rev. **119**, 348 (1960); H. Myers, A. Odian, P. C. Stein, and A. Wattenberg, *ibid.* **95**, 576 (1954); A. C. Odian, P. C. Stein, A. Wattenberg, B. T. Field, and R. Weinstein, *ibid.* **102**, 837 (1956); A. Wattenberg, A. C. Odian, P. C. Stein, H. Wilson, and R. Weinstein, *ibid.* **104**, 1710 (1956).
[5]K. Gottfried, Nucl. Phys. **5**, 557 (1958).
[6]J. Arends, J. Eyink, H. Hartmann, A. Hegerath, B. Mecking, G. Noldeke, and H. Rost, Z. Phys. A **298**, 103 (1980); H. Hartmann, H. Hoffman, B. Mecking, and G. Holdeke, in *Proceedings of the International Conference on Photo-Nuclear Reactions and Applications, Asilomar, 1973,* edited by B. L. Berman (Lawrence Livermore Laboratory, Livermore, 1973), pp. 967–976.
[7]S. Homma, M. Kanazawa, K. Maruyama, Y. Murata, H. Okuno, A. Sasaki, and T. Taniguchi, Phys. Rev. Lett. **45**, 706 (1980); S. Homma, M. Kanazawa, K. Maruyama, Y. Murata, H. Okuno, A. Sasaki, and T. Taniguchi, Phys. Rev. C **27**, 31 (1983).
[8]K. Baba, I. Endo, H. Fukuma, K. Inoue, T. Kawamoto, T. Ohsugi, Y. Sumi, T. Takeshita, S. Uehara, Y. Yano, and T. Maki, Nucl. Phys. **A415**, 462 (1984).
[9]O. Piccioni, D. Clark, R. Cool, G. Friedlander, and D. Kassner, Rev. Sci. Instrum. **26**, 232 (1955).
[10]S. Arai, S. Homma, A. Itano, T. Inagaki, M. Kasuya, K. Maruyama, T. Miyachi, H. Okuno, A. Sasaki, I. Sato, K. Ukai, and T. Yamakawa, Jpn. J. Appl. Phys. **14**, 95 (1975).
[11]T. Kitami, Y. Akino, S. Kato, H. Okuno, Y. Doi, and A. Masaike, Institute for Nuclear Study Report INS-TH-94, 1975.
[12]M. Sakuta, M. Sc. thesis, Kyoto University, 1978.
[13]The absolute values of the cross sections of the present experiment are smaller than the ones obtained by the previous experiment (Ref. 7) at the proton angle of 25°. The discrepancies range from 20% to 30% to almost a factor of 2, depending on the momentum of protons, and cannot be understood to be due to the difference in the measured angles. We examined the present and previous analyses in detail to find the sources of the discrepancy, and found that there was a misestimation in the spectrometer acceptance used in the analysis of the previous experiment. Although the overall features of the previous results seem to agree with the present results on applying the recalculated acceptance, it is not possible by now to correct each value of the previous cross sections point by point.
[14]See AIP Document No. PAPS PRVCA35-1828-8 for 8 pages of double differential cross sections of the reactions $\gamma + A = p +$ anything. Order by PAPS number and journal reference from American Institute of Physics, Physics Auxiliary Publication Service, 335 East 45th Street, New York, NY 10017. The prepaid price is $1.50 for a microfiche, or $5 for a photocopy. Airmail additional.
[15]J. Arends, H. J. Gassen, A. Hegerath, B. Mecking, G. Noldeke, P. Prenzel, T. Reichelt, A. Voswinkel, and W. W. Sapp, Universität Bonn Report BONN-HE-83-1, 1983.
[16]M. Kanazawa, Ph.D. thesis, University of Tokyo, 1985.
[17]G. Jacob and A. J. Maris, Rev. Mod. Phys. **45**, 6 (1973).
[18]M. Wakamatsu and K. Matsumoto, Nucl. Phys. **A392**, 323 (1983).
[19]S. Homma and H. Tezuka, J. Phys. Soc. Jpn. **55**, 780 (1986).
[20]J. Suzumura and Y. Futami, Prog. Theor. Phys. **68**, 2060 (1982).